ChemComm
Chemical Communications

Accepted Manuscript

This article can be cited before page numbers have been issued, to do this please use: R. Kushwaha, V. Singh, B. Koch and S. Banerjee, *Chem. Commun.*, 2025, DOI: 10.1039/D5CC03374H.

ROYAL SOCIETY OF CHEMISTRY

rsc.li/chemcomm

ChemComm

View Article Online
DOI: 10.1039/D5CC03374H

COMMUNICATION

Bexarotene-Attached Re(I) Tricarbonyl Complex for NADH Oxidation and ROS-mediated Cancer Phototherapy†

Received 00th January 20xx,
Accepted 00th January 20xx

DOI: 10.1039/x0xx00000x

Rajesh Kushwaha,[a] Virendra Singh,[b] Biplob Koch,*[b] and Samya Banerjee*[a]

An axially substituted polypyridyl Re(CO)₃ complex bearing bexarotene triggered caspase-3/7-mediated apoptosis in cancer cells through ROS generation and NADH photo-oxidation.

Photoactivated cancer therapy (PACT) has emerged as a promising anticancer strategy for achieving spatial and temporal control over cytotoxicity while minimizing off-target effects.[1] So far, the clinically used photosensitizers are built upon tetrapyrrolic scaffolds, e.g., phthalocyanine, porphyrin, etc., which control their photophysical as well as biological behaviour.[2] Due to these shared structural motifs, many of them exhibit similar limitations, including low water solubility, poor photostability, tedious synthesis/purification, and slow clearance, often leading to chronic photosensitivity.[2,3] To address these challenges, metal complexes caught attention due to the unique photophysical and photochemical properties, which can be finely tuned by ligand design and metal choice.[4] Moreover, transition metal complexes also possess high photostability, unique excited state activities, and redox behaviour for generating reactive oxygen species (ROS) and multimodal actions, such as NADH photo-oxidation.[5] In this regard, Re(I) tricarbonyl ($Re(CO)_3$) complexes have garnered a surge in interest as light-responsive anticancer agents owing to their long-lived excited states, and favorable photochemical/photophysical properties.[6] These complexes primarily operate via light-induced $^1O_2$ and other ROS generation to kill cancer cells selectively.[6] For example, Mao and co-workers developed carbonic anhydrase IX appended Re(I) Photosensitizer showing immunogenic anticancer potential.[7] The Wilson group has realized the light-responsive anticancer potential of a wide range of phenanthroline-based $Re(CO)_3$ complexes via ROS generation and CO toxicity.[8] Recently, our group has reported phenanthroline and terpyridine-based $Re(CO)_3$ complexes showing light-triggered anticancer activity via synergistic ROS generation and NADH photo-oxidation.[9] Zhang and co-workers also explored the light-activated ROS generation and NADH photo-oxidation mediated immunotherapeutic potential of phenanthroline-based $Re(CO)_3$ complexes.[10] Despite these advances, very limited $Re(CO)_3$ complexes demonstrating simultaneous ROS production and NADH photo-oxidation under visible light are reported, a combination that could synergistically disrupt mitochondrial function and trigger apoptotic pathways in cancer cells.[5] Moreover, the structural diversity of light-responsive $Re(CO)_3$ complexes has largely been restricted to modifications on α-diimine ligands or axial substitution with pyridine, isonitrile, or phosphine derivatives.[5,6,11] In this study, for the first time, we sought to explore the potential of carboxylate derivatives as axial substitutions in $Re(CO)_3$ complexes to open the scope for this class of photo-responsive $Re(CO)_3$ complexes in photoactivated cancer therapy. Successful implementation might allow the use of a wide range of bioactive/photoactive carboxylate derivatives as axial substituents. In addition, although RXR agonists have been explored in cancer therapeutics, their direct conjugation to a PACT agent and their impact on synergistic apoptosis pathways under light irradiation have also not been reported in $Re(CO)_3$ complexes.

We report two novel $[Re(CO)_3(N^N)L]$ complexes, **Re1** and **Re2**, incorporating bathophenanthroline as the diimine ligand (N^N), and either benzoic acid (**Re1**) or bexarotene (**Re2**) as axial ligands (L) (**Fig. 1a**). Benzoic acid was utilized as a control for biologically active bexarotene. Bexarotene, a clinically approved retinoid X receptor (RXR) agonist, is known for its established pro-apoptotic activity through modulation of gene expression and transcription factors.[12] In addition, bexarotene is also used in combination with other anticancer drugs to improve their efficacy and performance, making it a rational choice for additional bioactivity to the Re(I) scaffold.[12] Bathophenanthroline was used to exploit its extended π-conjugation and rigid planar structure to increase photosensitivity and excited states stabilization.[13]

[a]. *Department of Chemistry, Indian Institute of Technology (BHU), Varanasi, Uttar Pradesh 221005, India.*
[b]. *Department of Zoology, Institute of Science, Banaras Hindu University, Varanasi, Uttar Pradesh 221005, India.*
† *Electronic supplementary information (ESI) available. See*
DOI: 10.1039/x0xx00000x

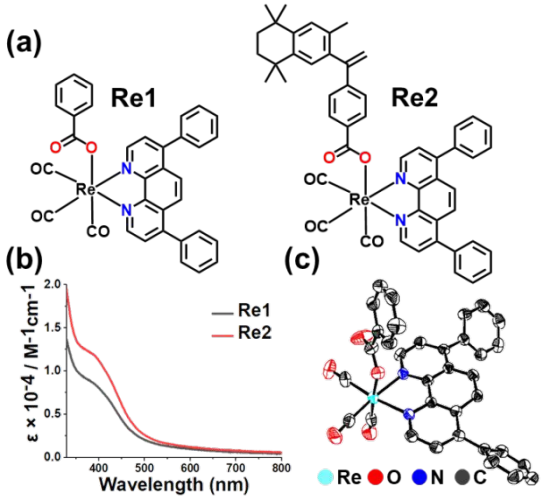

Fig. 1 (a) Structures of **Re1** and **Re2**. (b) UV-Vis. spectra of **Re1** and **Re2** in DMSO:H_2O (1:9 v:v). (c) X-ray structure of **Re1**.

Re1 and **Re2** were synthesized from the parent $[Re(CO)_3(N^N)Cl]$ complexes by substituting Cl with L (anionic benzoic acid (**Re1**); bexarotene (**Re2**)) in the presence of AgOTf, where N^N was bathophenanthroline (**Scheme S1, ESI†**). Complexes were characterized with several spectroscopic techniques (**Figs. S1-S8, ESI†**). In ^{1}H NMR, the peaks between 6.5-9.5 ppm were attributed to aromatic protons of **Re1**/**Re2**, and the peaks between 0.9-1.6 ppm and 4.9-5.7 ppm (in **Re2)** were attributed to alkyl group and unsaturated protons, respectively (**Figs. S1, S2 ESI†**). The presence of carbonyls in **Re1** and **Re2** was confirmed by the $^{13}C\{^1H\}$ NMR peaks observed between 185–200 ppm and by characteristic FT-IR bands between 1885–2020 cm^{-1} (**Figs. S3–S6, ESI†**). The HRMS spectra in MeOH displayed a molecular ion peak corresponding to $[M+H]^+$ (**Figs. S7, S8, ESI†**). The UV-Vis. spectra of **Re1** and **Re2** revealed an absorption band ~ 385 nm with an extended tail (up to 500 nm) in the visible region (**Fig. 1b**) across different pH (6-8) (**Fig. S9, ESI†**), suggesting their ability to absorb visible light (might be useful to induce light-triggered anticancer effect). **Re2** displayed weak emission at ~625 nm at 380 nm excitation (**Fig. S10, ESI†**). High photostability is crucial for any phototherapeutic to avoid photobleaching or off-target problems.[4] Interestingly, both complexes displayed excellent photostability up to 4 h, as evidenced by the insignificant change in NMR and UV-Vis. spectra (**Figs. S11, S12 ESI†**). **Re2** exhibited a log $P_{o/w}$ (octanol-water coefficient) value of +1.22 ± 0.12 (**Figs. S13, ESI†**), indicating its lipophilic nature.

Re1 was crystallized in the P121/n space of the monoclinic crystal system. **Re1** had a distorted octahedral shape featuring a ReC_3N_2O coordination core, with axial benzoate, three facial carbonyls, and two nitrogens of bathophenanthroline (**Figs. 1C, S14, ESI†**). The axial Re-O bond length was comparatively shorter than the axial Re-Cl bond length in the corresponding chloride complexes, indicating a stronger bond formation.[9,14] Selected crystallographic parameters and selected bond lengths/angles are provided in **Tables S1, S2**, **ESI†**, respectively. Furthermore, the computational studies were performed to get an insight into the electronic and photophysical behaviour of **Re1** and **Re2**. The complexes were optimized in their different state with CAM-B3LYP functional with combinatorial (LANL2DZ with pseudo LANL2 for Re and 6-31g* for other atoms) basis sets using Gaussian 16 (**Figs. 2a, S15, S16, ESI†**).[9] The analysis of FMOs revealed that the HOMOs of **Re1** and **Re2** were localized on $Re(CO)_3$ core with slight involvement of bexarotene in **Re2**, while the LUMOs of **Re1** and **Re2** were purely distributed on π* orbitals of bathophenanthroline (**Figs. S17, S18, ESI†**). The ΔEg = E_{LUMO}–E_{HOMO} for **Re2** was slightly lower than **Re1**, indicating better photo-sensitivity of **Re2** (**Table S3, ESI†**).[15] The energies of the ten singlet/triplet excited states were determined to understand the energy differences between the S_o and the corresponding excited S_n/T_n states (**Tables S4, S5**, **ESI†**). The intersystem crossing (ISC) efficiently occurs with a small energy gap ($\Delta E_{S1\text{-}Tn} < 0.3$ eV) between the S_1 and T_n states.[15] Thus, based on excitation energies analysis, the possible channels for ISC of **Re2** are given in **Fig. 2b**. The NTO analysis of these transitions indicated the involvement of ^{1}LLCT to ^{3}LLCT transitions (**Figs. 2c, S19, S20, ESI†**). The energy difference, ΔE_{S0-T1}, underlined the efficacy of the lowest-lying triplet state that has adequate energy to generate $^1O_2$ (i.e., > 0.98 eV) to proceed via the PDT type-II pathway (**Fig. 2b**). The SOMO plots and spin density plots at the triplet excited state of **Re1** and **Re2** (**Figs. S21, S22, ESI†**) revealed that the unpaired electrons are distributed around Re(I) and bathophenanthroline, indicating their mixed metal-ligand-based character.

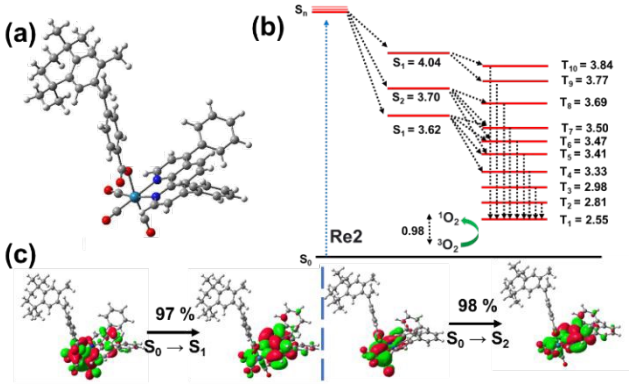

Fig. 2 (a) Optimized structure of **Re2** in ground state. (b) Calculated excited state energy and possible ISC channels of **Re2**, (energy in eV). (c) NTOs for $S_0 \rightarrow S_1/S_2$ transition for **Re2**.

The absorbance within the visible range, high photostability, and potent theoretical $^1O_2$ generation ability of **Re1** and **Re2** inspired us to investigate them as PACT agents. In PACT, $^1O_2$ production plays a critical role in causing oxidative stress, disrupting membranes, denaturing proteins, and damaging DNA.[1,6,8] The $^1O_2$ generation ability was determined using diphenyl isobenzofuron (DPBF) as a $^1O_2$ probe.[16] The absorbance of DPBF remained unchanged in the presence of **Re1** and **Re2** (**Fig. S23, ESI†**) under dark, indicating no detectable $^1O_2$ generation. However, there was a gradual decrease in DPBF-based absorption peaks when light (400-700 nm, 10 J cm^{-2}) was exposed, exhibiting $^1O_2$ generation (**Figs. 3a, S24, ESI†**), even under different pH conditions (**Figs. S25, ESI†**).

View Article Online
DOI: 10.1039/D5CC03774H

The $^1O_2$ quantum yield (Φ_Δ) of **Re1** and **Re2** was 0.12–0.14 with $[Ru(bpy)_3]Cl_2$ as standard (Φ_Δ = 0.22).[9] Kim group has reported that several photosensitizers capable of generating light-induced $^1O_2$ can also facilitate photocatalytic NADH oxidation.[17] NADH is a vital coenzyme that actively participates in the electron transport chain (ETC) and plays a crucial role in metabolism.[5,17,18] Thus, its oxidation can impair ETC function in cancer cells, ultimately leading to cell death.[5,18] The obtained results revealed that there was no notable change in NADH (150 µM) absorbance in the presence of **Re1** and **Re2,** indicating no oxidation of NADH (**Fig. S26, ESI†**) in the dark. Upon light (400-700 nm, 10 J cm^{-2}) exposure, the characteristic absorbance of NADH at *ca.* 339 nm gradually decreased; at the same time, the absorbance at *ca.* 256 nm corresponding to NAD^+ progressively increased in the presence of **Re1**/**Re2**, indicating the photo-oxidation of NADH to NAD^+ (**Figs. 3b, S27, ESI†**). Moreover, the NADH photo-oxidation ability of **Re2** did not change in the presence of different ROS scavengers (D-mannitol for radical-based ROS, and NaN_3 for $^1O_2$) (**Fig. S28, ESI†**), indicating ROS-independent **Re2**-mediated NADH photo-oxidation. The turnover frequency (TOF) for **Re2** (TOF = 13.6 h^{-1}) was comparatively higher than **Re1** (TOF = 9.0 h^{-1}) for NADH to NAD^+ oxidation. These findings suggested that **Re1**/**Re2** could act as a phototherapeutic agent that can produce ROS, such as $^1O_2$ and oxidize NADH upon light exposure.

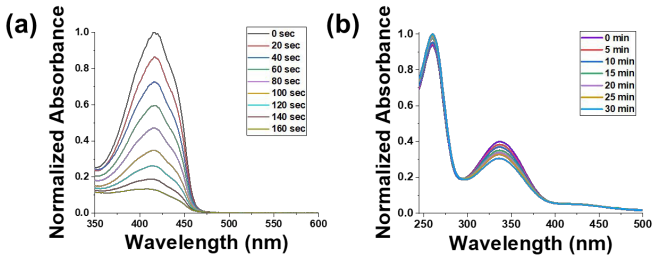

Fig. 3 (a) $^1O_2$ generation by **Re2** under light exposure in DMSO:PBS (2 : 98 v/v). (b) NADH photo-oxidation by **Re2** under light exposure in DMSO:PBS (2 : 98 v/v).

The ability of **Re1** and **Re2** to produce $^1O_2$ and oxidize NADH under light exposure prompted us to investigate their anticancer efficacy against A549 (Lung cancer), MCF-7 (breast cancer) cells, and normal HEK-293 (Human embryonic kidney) cells under both dark and light exposure. The dark and light IC_{50} values of **Re1** and **Re2** are provided in **Table S6**. **Re1** and **Re2** exhibited minimal cytotoxic effect against both lung (IC_{50} > 50 µM for **Re1** and ~36 µM for **Re2**) and breast (IC_{50} = ~21 µM for **Re1** and ~19 µM for **Re2**) cancer cells under dark conditions (**Figs. S29-S32 ESI†**). However, their cytotoxicity was notably improved upon light exposure as the IC_{50} for **Re2** was found to be ~0.27 and ~1.02 µM against MCF-7 and A549 cells, respectively. While IC_{50} for **Re1** was found to be ~3.91 and 12.01 µM against MCF-7 and A549 cells, respectively. The phototoxicity index (PI = dark IC_{50}/light IC_{50}) of **Re2** (PI up to 71) was much higher than **Re1** (PI up to 5.6), possibly due to its higher $^1O_2$ generation/NADH photo-oxidation efficacy. Importantly, **Re1** and **Re2** did not exhibit cytotoxicity (IC_{50} > 50 µM) towards normal HEK-293 cells, irrespective of light or dark conditions (**Figs. S33, S34 ESI†**), aligning well with the clinical rationale of photosensitizers. This result indicated that **Re2** selectively killed cancer cells without harming normal cells with a high selectivity index (SI = light $IC_{50\ normal\ cells}$/light $IC_{50\ cancer\ cells}$) of up to 185. The High selectivity of **Re2** can be attributed to the RXR targeting nature of the appended bexarotene motif.[12] To gain insight into the effect of bexarotene on the $Re(CO)_3$ complex, molecular docking study was performed with **Re1**, **Re2**, and bexarotene with the RXRα receptor (PDB ID: 1MVC) (**Fig. S35, ESI†**).[19] The docking results **(Table S7, ESI†)** suggested an improvement in RXRα receptor-binding capability of **Re2**. Furthermore, the interaction analysis revealed that both **Re2** and Bexarotene formed similar hydrogen bonds with ARG A:316 of the RXRα receptor, a key residue involved in RXRα activation and increased hydrophobic interaction within the RXRα receptor's binding pocket (**Figs. S36-S38, ESI†**).

For cell death mechanistic studies, the DCFH-DA (2,7-dichlorodihydrofluorescein diacetate) assay was used to determine in-cell ROS generation in MCF-7 cells.[9,20] The obtained result revealed that **Re2** caused significant in-cell ROS generation in MCF-7 cells after light (400-700 nm, 10 J cm^{-2}) exposure, as indicated by bright green fluorescence in **Fig. 4a**. In contrast, **Re2** alone (dark conditions) did not induce notable ROS production, reaffirming its light-dependent ROS-generating capability (**Fig. 4a**). Previous reports suggested that the photosensitizers showing light-triggered ROS production and NADH photo-oxidation can effectively disrupt MMP (mitochondrial membrane potential) and trigger apoptosis in cancer cells.[5,9] Hence, we assessed the change in MMP of **Re2**-treated MCF-7 cells under light and dark by JC-1 assay (**Fig. 4b**). In this method, the JC-1 dye accumulates in mitochondria and displays red emission at higher MMP, whereas at lower MMP, it displays green emission and gets dispersed in the cytoplasm. Under dark, **Re2**-treated MCF-7 cells displayed red emission, revealing no notable MMP alternation (**Fig. 4b**). In contrast, **Re2**-treated MCF-7 cells displayed green emission following the light (400–700 nm, 10 J cm^{-2}) exposure, reflecting a significant loss and change in MMP (**Fig. 4b**). Thus, **Re2** effectively altered the MMP of MCF-7 cells under light rather than dark conditions. The change in MMP of **Re2**-treated A549 cells under light exposure suggests a higher probability of mitochondrial damage triggering apoptosis.[20,21] Thompson and coworkers have shown a direct correlation between mitochondrial integrity, MMP, and apoptosis.[20] Also, Bexarotene derivatives are known to induce apoptosis in cancer cells.[12] Hence, the mechanism of cell death induced by **Re2** was investigated in A549 cells by AO (Acridine Orange)/EtBr (Ethidium Bromide) staining.[20] As shown in **Fig. 4c**, MCF-7 cells treated with **Re2** or dark/light only exhibited a well-organized cytoplasm and intact green-stained nuclei, indicating that **Re2** is mostly non-toxic under dark conditions. However, light-exposed **Re2**-treated MCF-7 cells produced bright green/yellowish nuclei along with membrane blebbing, indicating the occurrence of early and late apoptosis. Annexin V-FITC/PI dual staining assay revealed that the controls and **Re2** under dark conditions presented negligible cell death. However, under **Re2**+light treatment, the cell death

was notably increased, with *ca*. 10 % early apoptosis, 31 % late apoptosis, and 25% necrosis (**Fig. S39, ESI†**). Caspase 3/7 are the key executioner of apoptosis, and their activation ultimately results in programmed cell death.[18] The potential of **Re2** for caspase activation was determined in A549 cells using caspase 3/7 and SYTOX red assay.[20] The result revealed that the only **Re2**+light-treated group demonstrated caspase 3 activation (**Fig. S40, ESI†**). Based on these findings, it could be concluded that **Re2** caused ROS generation and NADH photooxidation under light exposure that compromised MMP and executed Caspase-3/7 activation to induce apoptosis in MCF-7 cells.

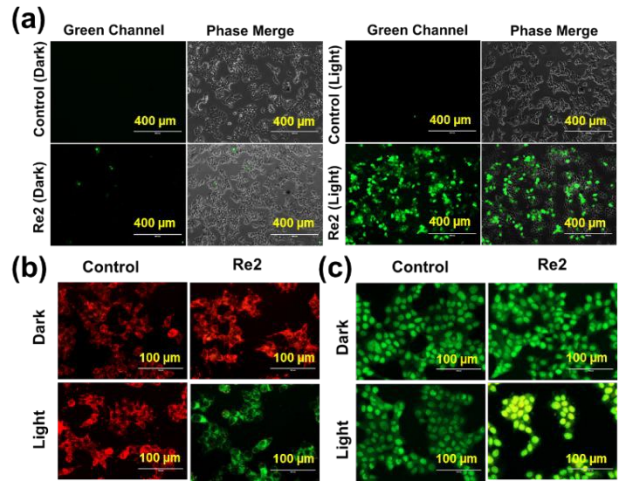

Fig. 4 (a) ROS generation induced by **Re2** in MCF-7 cells. Scale bar = 400 µm. (b) Mitochondrial depolarization induced by **Re2** in MCF-7 cells. Scale bar = 100 µm. (c) AO/EtBr assay indicating apoptosis in MCF-7 cells induced by **Re2**. Scale bar = 100 µm.

Overall, we report two $Re(CO)_3$ complexes (**Re1** and **Re2**) featuring bathophenanthroline as a diimine ligand and either benzoate (**Re1**) or bexarotene (**Re2**) as axial carboxylate ligands. Upon light exposure, these complexes induced the oxidation of NADH to NAD^+ and generated $^1O_2$, thereby activating dual mechanisms of cancer cell death. **Re2** demonstrates potent photocytotoxicity against A549 and MCF-7 cancer cells via ROS-mediated mitochondrial dysfunction and caspase-3/7-dependent apoptosis while sparing normal HEK 293 cells. This work highlights the phototherapeutic potential of integrating an axial carboxylate bioactive ligand with a photoactive Re(I) scaffold to develop next-generation phototherapeutic agents for photoactivated cancer therapy.

This work was supported by the SERB (now ANRF), India (SRG/2022/000030), India. R.K. thanks the GOI for the PMRF. R. K. performed synthesis, characterisation, in-solution studies, X-ray crystallography, TD-DFT calculations, and MD studies. V. S. and B. K. performed the biological studies. S. B. formulated the concept and overall project.

Conflicts of interest

There are no conflicts to declare.

Data availability

The data supporting this article have been included as part of ESI†.

View Article Online
DOI: 10.1039/D5CC03374H

References

1 (a) H. Shi and P. J. Sadler, *Angew. Chem. Int. Ed.*, 2025, **64**, e202423335; (b) K. M. Kuznetsov, K. Cariou and G. Gasser, *Chem. Sci.,* 2024, **15**, 17760-17780.
2 (a) B. Zheng, Q. He, X. Li, J. Yoon and J. Huang, *Coord. Chem. Rev.,* 2021, **426**, 213548; (b) W. Yina, P. Lib, H. Huang, L. Fengb, S. Liub, X. Liu and F. Bai, *RSC Adv.,* 2024, **14**, 29368-29383.
3 X. Zhao, J. Liu, J. Fan, H. Chao and X. Peng, *Chem. Soc. Rev.,* 2021, **50**, 4185-4219.
4 (a) J. Karges, *Angew. Chem. Int. Ed.,* 2022, **61**, e202112236; (b) S. A McFarland, A. Mandel, R. Dumoulin-White and G. Gasser, *Curr. Opin. Chem. Biol.* 2020, **56**, 23–27; (c) L. Skos, Y. Borutzki, C. Gerner, S. M. Meier-Menches, *Curr. Opin. Chem. Biol.,* 2023, **73**, 102257.
5 A. K. Yadav, R. Kushwaha, A. A. Mandal, A. Mandal and S. Banerjee, *J. Am. Chem. Soc.,* 2025, **147**, 7161–7181.
6 (a) K Schindler and F Zobi, *Molecules*, 2022, **27**, 539; (b) A. S. S, V. N. B. Kar, U. Das and P. Paira, *RSC Adv.*, 2022, **12**, 20264-20295; (c) R. Kushwaha and S. Banerjee, *Fut. Med. Chem.,* 2025, **17**, 1101-1103.
7 X. Su, W. Wang, Q. Cao, H. Zhang, B. Liu, Y. Ling, X. Zhou and Z. Mao, *Angew. Chem. Int. Ed.*, 2022, **61**, e202115800.
8 (a) K. M. Knopf, B. L. Murphy, S. N. MacMillan, J. M. Baskin, M. P. Barr, E. Boros and J. J. Wilson, *J. Am. Chem. Soc.,* 2017, **139**, 14302–14314; (b) S. C. Marker, A. P. King, R. V. Swanda, B. Vaughn, E. Boros, S. Qian and J. J. Wilson, *Angew. Chem. Int. Ed.,* 2020, **59**, 13391-13400.
9 (a) R. Kushwaha, V. Singh, S. Peters, A. K. Yadav, T. Sadhukhan, B. Koch and S. Banerjee, *J. Med. Chem.,* 2024, **67**, 6537–6548; (b) R. Kushwaha, A. Upadhyay, S. Saha, A. K. Yadav, A. Bera, A. Dutta and S. Banerjee, *Dalton Trans.*, 2024, **53**, 13591-13601.
10 D. Li, G. Wen, H. Wang, Q. Ren, D. Wang, A. Dao, H. Huang and P. Zhang, *J. Med. Chem.,* 2025, **68**, 3749-3763.
11 (a) L. C. Lee and K. K. Lo, *J. Am. Chem. Soc.* 2022, **144**, 14420-14440; (b) B. Kar, U. Das, N. Roy and P. Paira, *Coord. Chem. Rev.,* 2023, **474**, 214860.
12 D. Shen, X. Yu, Y. Wu, Y. Chen, G. Li, F. Cheng and L. Xia, *Expert Rev. Anticancer Ther*., 2018, **18**, 487-499; (b) L. T. Farol and K. B. Hymes, *Expert Rev. Anticancer Ther.,* 2004, **4**, 180–188.
13 A. C. Hachey, D. Havrylyuk and E. C. Glazer, *Curr. Opin. Chem. Biol*., 2021, **61**, 191-202.
14 B. Machura, M. Wolff, M. Jaworska, P. Lodowski, E. Benoist, C. Carrayon, N. Saffon, R. Kruszynski and Z. Mazurak, *J. Organomet. Chem.*, 2011, **696**, 3068-3075.
15 G. Xu, C. Li, C. Chi, L. Wu, Y. Sun, J. Zhao, X.-H. Xia and S. Gou, *Nat. Commun.*, 2022, **13**, 3064.
16 A. Linero-Artiaga, L. Servos, V. Rodríguez, J. Ruiz and J. Karges, *J. Med. Chem.* 2025, **68**, 7792−7806.
17 M. Li, Y. Xu, Z. Pu, T. Xiong, H. Huang, S. Long, S. Son, L. Yu, N. Singh, Y. Tong, J. L. Sessler, X. Peng and J. S. Kim, *Proc. Natl. Acad. Sci. U. S. A.*, 2022, **119**, e2210504119.
18 A. Chiarugi, C. Dölle, R. Felici and M. Ziegler, *Nat. Rev. Cancer*, 2012, **12**, 741–752.
19 (a) G. M. Morris, R. Huey, W. Lindstrom, M. F. Sanner, R. K. Belew, D. S. Goodsell, A. J. Olson, J. Comput. Chem., 2009, 16, 2785-91. (b) Y. N. Nosova, D. S. Karlov, S. A. Pisarev, I. A. Shutkov, V. A. Palyulin, M. Baquié, E. R. Milaeva, P. J. Dyson, A. A. Nazarov, *J. Organomet. Chem.* 2017, **839**, 91–97.
20 A. Mandal, V. Singh, S. Peters, A. A. Mandal, T. Sadhukhan, B. Koch and S. Banerjee, *Dalton Trans.*, 2025, **54**, 6785–6789.
21 E. Gottlieb, S. Armour, M. H. Harris and C. B. Thompson, *Cell Death Differ.,* 2003, **10**, 709−717.

View Article Online
DOI: 10.1039/D5CC03374H

Data availability

The data supporting this article have been included as part of ESI†.